BMC Pulmonary Medicine

RESEARCH

Open Access

CT-Based radiomics nomogram of lung and mediastinal features to identify cardiovascular disease in chronic obstructive pulmonary disease: a multicenter study

XiaoQing Lin[1,2†], TaoHu Zhou[1†], Jiong Ni[3], XiuXiu Zhou[1], Yu Guan[1], Xin'ang Jiang[1], Yi Xia[1], FangYi Xu[4,5], HongJie Hu[4,5], Jie Li[1,2], Jin Zhang[1], Shiyuan Liu[1], Rozemarijn Vliegenthart[6] and Li Fan[1*]

Abstract

Rationale and objectives To investigate the performance of two diagnostic models based on CT-derived lung and mediastinum radiomics nomograms for identifying cardiovascular disease (CVD) in Chronic Obstructive Pulmonary Disease (COPD) patients.

Materials and methods Hospitalized participants with COPD were retrospectively recruited between September 2015 and April 2023. Clinical data and visual coronary artery calcium score (CACS) were collected. Radiomics features of lung and mediastinum were extracted. Least absolute shrinkage and selection operator (LASSO) logistic regression was applied for feature selection and radiomic model construction. We constructed 3 radiomics models, based on lung, mediastinum, and combined lung-and-mediastinum. Multivariate logistic regression model was used to establish radiomics nomograms. The performance of radiomics nomograms was evaluated by area under the ROC curve (AUC) and decision curve analysis (DCA).

Results Of 686 COPD patients, 131 had a history of CVD. Age, neutrophilic granulocyte percentage, hematocrit and GOLD stage were independent clinical factors for CVD. 12 lung, and 6 mediastinum radiomic features were collected to construct the radiomics models. As the lung-and-mediastinum radiomics model included the same 6 features as the mediastinum model, finally 2 radiomics models were studied (lung, mediastinum). The 2 radiomics nomograms showed better discriminatory ability (AUC: 0.79, 95%CI [0.72, 0.86] for lung; 0.86, 95%CI [0.81, 0.92]) for mediastinum) than the clinical factors model (AUC: 0.71, 95%CI [0.64, 0.78]) and visual CACS (AUC: 0.65, 95%CI [0.57, 0.72]). DCA demonstrated the 2 radiomics nomograms outperformed the clinical factors and CACS across the majority of the range of reasonable threshold probabilities.

Conclusion We developed chest CT-based nomograms to identify CVD in COPD patients, in particular based on mediastinum features, had better discriminatory power than clinical factors and visual CACS.

†XiaoQing Lin and TaoHu Zhou contributed equally to this work.

*Correspondence:
Li Fan
fanli0930@163.com

Full list of author information is available at the end of the article

Trial registration This retrospective study was approved by the institutional review boards at Second Affiliated Hospital of Naval Medical University, Tongji Hospital of Tongji University and Sir Run Run Shaw Hospital (ChiCTR2300069929 March 29, 2023). Retrospectively registered.

Key Results
The 2 nomograms for identifying CVD in COPD patients were constructed.
The 2 nomograms showed better discriminatory ability than the clinical model.
The AUC of mediastinum nomogram was significantly better than for lung.

Keywords Chronic obstructive pulmonary disease (COPD), Cardiovascular disease, Computed tomography (CT), Radiomics, Coronary artery calcium (CAC)

Introduction

Chronic obstructive pulmonary disease (COPD) is a leading cause of morbidity worldwide, and is the third leading cause of death [1]. The prevalence of COPD was reportedly 8.6% among adults aged 20 years and above, and 13.7% among adults older than 40 years in China [2]. The COPD burden in China may substantially elevate in the next decades because of increasing smoking rates and an aging population, accounting for 32% of the global economic burden [3]. Comorbidities are widespread in COPD patients, among which Cardiovascular Disease(CVD) is the most common one [4]. The cardiac and pulmonary functions are physiologically integrated. Previous studies showed that the volume of intrathoracic air is closely related to the tension of the left ventricular wall. The impairment of cardiac function in COPD patients is largely caused by mechanical factors of lung hyperinflation [5]. Furthermore, smoking, aging, and inflammation are common factors and mechanisms linking these two diseases [6]. Nearly half of all hospitalizations and deaths in COPD patients are attributable to CVD [7]. Conversely, the presence and progression of CVD may trigger acute exacerbations of COPD [1]. Due to the close relationship between the two diseases, it is important to diagnose coexisting CVD early in COPD patients.

Previous studies to predict CVD were proposed based on demographic and clinical variables [8, 9]. Nevertheless, the QRISK3 score tool (incorporating parameters such as race, age, gender, and medical history), widely used in the United Kingdom and other countries, has been shown to underestimate the risk of CVD in COPD patients [10]. Chest CT imaging plays an important role in the evaluation of patients with COPD; this may provide the opportunity to detect (early stages of) CVD, for example based on radiomics. Radiomics is used to convert medical images into high-dimensional data through high-throughput quantitative feature extraction and later data analysis to support decision-making [11]. In prior reports, radiomics models in imaging were developed to identify chest diseases [12–14]. In our previous study, a whole-lung radiomics nomogram was shown to be able to identify CVD in COPD patients [15]. However, the mediastinum, including the structure of the cardiovascular system itself, may have better discriminatory power. To the best of our knowledge, the value of CT-based mediastinum radiomics models for CVD identification in chest CT has not been previously studied. In addition, noninvasive indicators for cardiovascular disease, such as coronary artery calcification (CAC) detected on CT imaging, have demonstrated superior risk assessment capabilities compared to traditional scoring systems in the general population [16]. A previous study demonstrated limited effectiveness in predicting CVD in patients with COPD using visual scoring of CAC; the C-indexes of the Weston score and the Agatston score were 0.62 and 0.61, respectively [17]. We questioned whether the radiomics nomograms would have greater value to identify CVD in COPD patients compared to a visual score for CAC based on chest CT. The aim of this study was to compare the value of radiomics nomograms (radiomics plus clinical risk factors) of the lung and mediastinum to identify CVD in COPD patients.

Materials and methods

Patients and clinical data

This retrospective study was approved by the institutional review boards at Second Affiliated Hospital of Naval Medical University, Tongji Hospital of Tongji University and Sir Run Run Shaw Hospital (ChiCTR2300069929; March 29, 2023); no patient informed consent was needed because it was a retrospective study. This study is a secondary analysis of existing data. From September 2015 and April 2023, 974 hospitalized patients with confirmed COPD based on pulmonary function tests (PFT) at three centers were enrolled from the CSD-COPD cohort. Inclusion criteria were: (1) COPD confirmed by PFT; (2) PFT and chest CT within 2 weeks; (3) Complete thin-slice (1 mm) chest CT images. Exclusion criteria were: (1) Co-morbid other thoracic disease (e.g., pneumonia, pulmonary atelectasis, lung nodule or mass and pleural effusion); (2) Known with any malignant tumors. (3) Coronary stents or coronary artery bypass grafting or cardiac implants, or other mediastinal surgery. (4) Spine

implants or marked image artifacts. The flowchart of patient selection is shown in Fig. 1. Finally, 686 subjects were included in the study. Among them, 468 subjects from Second Affiliated Hospital of Naval Medical University and Sir Run Run Shaw Hospital were randomized as training ($n = 328$) or internal validation cohort ($n = 140$) with the ratio of 7:3. Subjects from Tongji Hospital of Tongji University were classified as independent external validation cohort ($n = 218$). Description of the sample size can be found in the Supplementary Material.

Clinical information was obtained based on electronic medical records, including age, weight, height, body mass index (BMI), gender, GOLD stage, smoking status, smoking index (smoking index = smoking years × daily smoking volume (Number of cigarettes)), hypertension, diabetes, hypercholesterolemia. For blood laboratory testing as part of routine check during hospitalization, we included assessments if obtained in at least 70% of the participants; these assessments were white blood cell count, neutrophilic granulocyte percentage, percentage of lymphocytes, absolute eosinophil count, hematocrit, globulin, red blood cell distribution width and mean platelet volume. In case of missing values, blood test results and smoking index (missing 3.8%) were filled with the mean. For the rationale behind using the mean value, refer to the Supplementary Material. CVD events were diagnosed by examination during hospitalization, and the interval between the CVD examination and the acquisition of the chest CT scan was less than one month. CVD events were defined, using the international classification of disease (ICD) 11 (https://icd.who.int/browse/2024-01/mms/en) definitions, as all diagnoses of Coronary artery disease(CAD, BA81-8Z) (Angina(BA40-4Z), (sub)acute myocardial infarction(BA41-60), acute or chronic ischaemic heart diseases(BA40-6Z)), cerebrovascular events (ischemic stroke(8B11), haemorrhagic stroke(8B00), and transient ischemic attack(8B10)), arrhythmia(BC80-9Y) and heart failure(BD10-1Z), which was determined based on hospitalization records and examinations. Importantly, we excluded patients with more easily identifiable signs of CVD on chest CT, namely enlarged heart chambers, history of coronary stenting and bypass grafting.

CT image acquisition and pulmonary function testing

Inspiration, expiration and breath-hold training were performed before the CT examination. The patient was in the supine position with both arms raised above the head, and axial CT images of the entire chest were obtained at the end of full inspiration. Table S1(supplement) shows the chest CT acquisition parameters in detail. PFT was

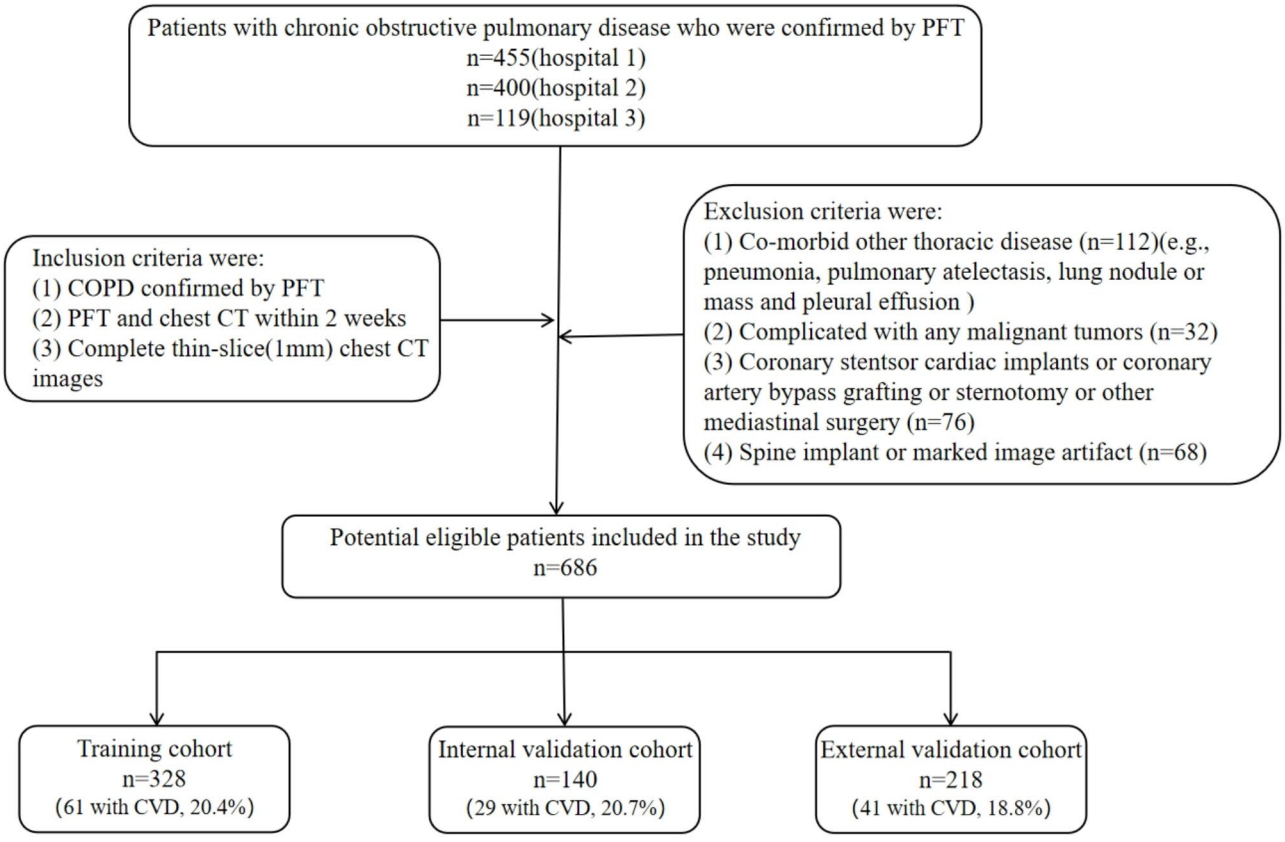

Fig. 1 Flowchart of patient selection

performed using CHEST Multifunction Spirometer HI-801 (Japan). Forced expiratory volume in one second (FEV1), percent predicted of forced expiratory flow in one second (FEV1%) and FEV1/FVC were measured. We applied the common diagnostic criteria for COPD: FEV1/FVC<0.7, and/or FEV1 increase less than 200 ml after the use of a bronchodilator [18]. Patients were grouped according to the global initiative for chronic obstructive lung disease [19]: GOLD I, FEV1/FVC < 0.7, FEV1 ≥ 80%; GOLD II, FEV1/FVC < 0.7, 80% < FEV1 ≤ 50%; GOLD III, FEV1/FVC < 0.7, 50%< FEV1 ≤ 30%; GOLD IV, FEV1/FVC < 0.7, FEV1 < 30%.

Visual coronary artery calcium score (CACS)

Two radiologists with 10 years of chest CT experience performed visual coronary artery calcium (CAC) scoring using an ordinal scale from 0 to 3 [20]; uncertain scores were checked by another radiologist with more than 15 years of chest CT experience to derive consensus. A score of 0 was assigned for no CAC, 1 for mild CAC, 2 for moderate CAC, and 3 for severe CAC. If there were only isolated flecks of CAC within a segment, it was classified as mild CAC. If continuous CAC was present within a segment, it was classified as severe CAC. Coronary calcifications were classified as moderate if they were more in number than mild coronary calcifications but less than severe coronary calcifications. Figure 2 shows an example of a standard set of images to demonstrate the scale. The consistency between 2 radiologists' CACS was assessed using kappa.

Whole lung and mediastinum segmentation

Whole lung segmentation was performed as follows. A publicly accessed deep-learning model, U-net (R231) (https://github.com/JoHof/lungmask), automatically segmented the right lung and left lung. The U-net (R231) model was trained on the publicly available lung CT dataset (R-36) with 231 cases selected for training, and tested on the publicly available datasets with 191 cases (VISCERAL Anatomy3 (VISC-36), LTRC (LTRC-36) and LCTSC (LCTSC-36)). Hyperparameters included a learning rate of 0.001, batch size of 8, with Dice Loss as the loss function and Adam as the optimizer. During training, the images were augmented by random rotation, non-linear deformation, and Gaussian noise [12]. The extracted left and right lung were merged into a combined region of interest (ROI). The automatic whole lung segmentation performance was verified in a previous study [21], and the mean Dice coefficient of whole lung segmentation using U-net (R231) was reported to be 0.97 ± 0.06.

Mediastinum segmentation comprised the following three steps: surrounding organs segmentation, coarse mediastinum segmentation, refined segmentation via U-net. Organs surrounding the mediastinum, such as pulmonary tissue, ribs, vertebrae, esophagus, trachea, stomach, liver, spleen and pancreas were firstly segmented via the public network TotalSegmentator [22]. This model was trained on a large dataset containing over 1000 CT scans with annotations for 104 anatomical structures. The annotated dataset (https://doi.org/10.5281/zenodo.6802613) and toolkit (https://www.github.com/wasserth/TotalSegmentator) are publicly availab le. A hull region was generated around the pulmonary border and through subtraction, dilation, erosion and blacktop hat operation among above-mentioned organs and hull region, the mediastinum part, was maintained, resulting in a coarse segmentation of the mediastinum. A radiologist with ten years of chest CT experience refined the segmentation and set beginning and end border of mediastinum for 200 cases to train a traditional 3D U-net, removing some trivial parts, e.g. tissues between neighboring vertebrae. Ground truth for refined mediastinum segmentation 3D U-net were the regions reviewed by radiologists. The custom 3D U-net was trained with a learning rate of 0.001, a batch size of 5, and a total of 800 epochs. These hyperparameters were empirically determined to achieve a balance between training speed and model performance. Since manual segmentation

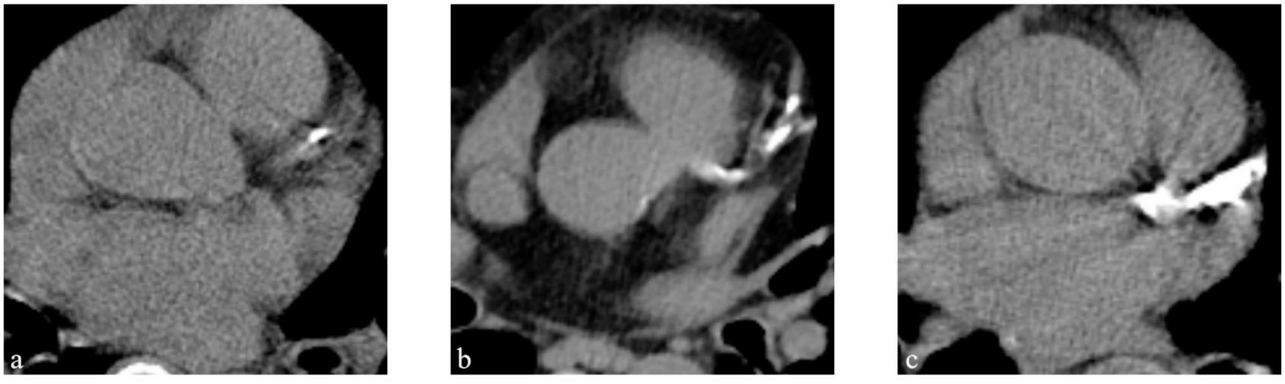

Fig. 2 Three examples of CAC score. (**a**) mild CAC, score of (1) (**b**) moderate CAC, score of (2) (**c**) severe CAC, score of 3.)

is often regarded as the ground truth, we assessed the consistency between manual and fully automatic mediastinum segmentation in 20 randomly selected patients. Radiologists with 10-year experience in chest radiology used ITK-SNAP software (version 3.8.0, www.itksnap.org) manually segmented 20 CT scans. The consistency between manual and fully automatic segmentation was assessed using the Dice index, an objective metric capable of quantifying the spatial overlap between two contours.

Radiomic features extraction

Before feature extraction, the images underwent a three-step preprocessing operation, voxel resampling, gray discretization, and image intensity normalization, resampling the image to $1 \times 1 \times 1$ mm, and adjusting the gray value of the image to 25 Gray levels, which is helpful to reduce the influence of different layer thickness and reduce the interference of noise. Then, Radiomics features were extracted using the open-source software Pyradiomics (3.0.1 version, https://pyradiomics.readthedocs.io/en/latest/), with three groups of features obtained: first-order, shape, and texture features. Radiomics features were extracted using Z-score normalization. The features of the lung-and-mediastinum model were based on the combination of features from the lung model and from the mediastinum model.

Radiomics feature selection and model construction

The best radiomics features were selected through the following two steps. First, the maximal redundancy minimal relevance (mRMR) algorithm was performed on the data of the training group to eliminate redundant and irrelevant parameters, and the number of features was reduced to 30 [12]. The optimal regularization parameter lambda was selected with the help of 10 cross-validations: a T-test was used to eliminate insignificant features ($p < 0.05$) and duplicate features with a Pearson correlation coefficient greater than 0.9 were excluded, and a LASSO regression analysis was implemented to achieve feature dimensionality reduction. The optimal regularization parameter, lambda, was finally determined. Parameters with feature coefficients which were not zero were used as the features of the finally constructed radiomics prediction model. No separate feature selection is performed on the external validation cohort. Finally, LASSO logistic regression coefficient was used to calculate the rad-score by weighting the sum of the products of the selected features and their respective corresponding coefficients, and the radiomics models based on rad-scores were constructed.

3 types of models were constructed, including the clinical model, radiomics model, and combined model (based on the best radiomics features and clinical factors). A nomogram was generated for visualization of the final combined model, graphical evaluation of variable importance and calculation of identification accuracy. The model training code is available in the Supplementary Material.

Subgroup analyses

The COPD population in the external validation cohort was grouped according to GOLD stage I-II and III-IV to validate the stability of the model across clinical subsets.

Statistical analysis

In this study, R software (version 4.2.2; http://www.Rproject.org) and IBM SPSS Statistics (version 26.0; IBM Corp., New York, USA) were used for statistical analysis and graphic production. Fisher's exact test or the chi-square test was used for discrete variables, and Mann-Whitney U test was used for continuous variables to compare patient characteristics. Univariate logistic regression analysis was used to obtain statistically significant risk variables, and then multivariate analysis was used to establish the clinical model and combined model. Univariate logistic regression analysis results with $p < 0.1$ were included in multivariate logistic regression analysis, and multivariate logistic regression analysis results were based on the Akaike information criterion (AIC). Calibration curves were used to determine the degree of agreement between predicted probabilities and observed results. Hosmer-Lemeshow test and decision curve analysis (DCA) was used to assess clinical validity. Area under the ROC curve (AUC) was used to analyze and evaluate the prediction performance of the model. The AUCs of different models were compared by Delong test. $P < 0.05$ was considered indicative of a statistically significant difference.

Results

Patient clinical factors and visual CACS models establishment

Table 1 displays the clinical factors of the patients. Out of 686 patients, the three hospitals included 423, 45, 218 patients, respectively. Mean age of the entire cohort was 69 years ± 10[SD], 130 were female. There were 555 COPD patients without CVD and 131 COPD patients with CVD. The number of cases with coronary artery disease, stroke, heart failure and arrhythmia in the three hospitals was 35, 4, 15 and 10; 26, 9, 0 and 6; 15, 0, 8 and 3, respectively.

Table 2 displays results of univariate and multivariate logistic regression. Based on the result of univariate logistic regression analysis, age, neutrophilic granulocyte percentage, hematocrit, GOLD stage and visual CACS were included in the multivariate analysis for further variable screening.

Table 1 Baseline characteristics of the study population

Clinical Factors		Training cohort (*n* = 328)			Internal validation cohort (*n* = 140)			External validation cohort (*n* = 218)		
		COPD without CVD (*n* = 267)	COPD with CVD (*n* = 61)	*P* value	COPD without CVD (*n* = 111)	COPD with CVD (*n* = 29)	*P* value	COPD without CVD (*n* = 177)	COPD with CVD (*n* = 41)	*P* value
Age		67.4 ± 9	70.3 ± 10.1	0.026	66.6 ± 10.6	72.8 ± 8.2	0.003	69.8 ± 10.2	69.6 ± 7.9	0.919
Gender				0.680			1.000			0.514
	Male	219 (82.0)	52 (85.2)		86 (77.5)	22 (75.9)		142(80.2)	35(85.4)	
	Female	48 (18.0)	9 (14.8)		25 (22.5)	7 (24.1)		35(19.8)	6(14.6)	
Height		163.3 ± 7.5	164.6 ± 8.2	0.212	163.2 ± 7.1	163 ± 10.3	0.934	164.3 ± 8.6	166.1 ± 6.3	0.135
Weight		63.3 ± 11	65.4 ± 13.3	0.197	62.6 ± 11.2	62.5 ± 12.3	0.981	64.5 ± 12.2	68.1 ± 14.1	0.095
BMI		23.7 ± 3.5	24.1 ± 4.1	0.476	23.5 ± 3.8	23.5 ± 3.6	0.988	23.9 ± 4.0	24.6 ± 4.5	0.293
GOLD stage				0.002			0.304			0.041
	GOLD I	63 (23.6)	8 (13.1)		28 (25.2)	3 (10.3)		35(19.8)	4(9.8)	
	GOLD II	148 (55.4)	31 (50.8)		58 (52.3)	19 (65.5)		84(47.5)	14(34.1)	
	GOLD III	44 (16.5)	22 (36.1)		18 (16.2)	6 (20.7)		41(23.2)	17(41.5)	
	GOLD IV	12 (4.5)	0 (0.0)		7 (6.3)	1 (3.4)		17(9.6)	6(14.6)	
Visual CAC score				<0.001			0.035			0.026
	0 (No)	163 (61.0)	23 (37.7)		60 (54.1)	13 (44.8)		104 (58.8)	14 (34.1)	
	1 (Mild)	66 (24.7)	15 (24.6)		30 (27.0)	6 (20.7)		44 (24.9)	16 (39.0)	
	2(Moderate)	34 (12.7)	20 (32.8)		19 (17.1)	6 (20.7)		22 (12.4)	10 (24.4)	
	3 (Severe)	4 (1.5)	3 (4.9)		2 (1.8)	4 (13.8)		7 (4.0)	1 (2.4)	
Hypertension				0.361			0.313			<0.001
	No	216 (80.9)	53 (86.9)		92 (82.9)	21 (72.4)		136 (76.8)	14 (34.1)	
	Yes	51 (19.1)	8 (13.1)		19 (17.1)	8 (27.6)		41 (23.2)	27 (65.9)	
Hyperlipidemia				1.000			0.206			0.001
	No	266 (99.6)	61 (100.0)		110 (99.1)	27 (93.1)		173 (97.7)	34 (82.9)	
	Yes	1 (0.4)	0 (0.0)		1 (0.9)	2 (6.9)		4 (2.3)	7 (17.1)	
Diabetes				0.672			1.000			0.012
	No	252 (94.4)	59 (96.7)		106 (95.5)	28 (96.6)		164 (92.7)	324 (78.0)	
	Yes	15 (5.6)	2 (3.3)		5 (4.5)	1 (3.4)		13 (7.3)	9 (22.0)	
Smoking status				0.498			0.463			0.267
	Never	143 (53.6)	37 (60.7)		59 (53.2)	12 (41.4)		113 (63.8)	21(51.2)	
	Current	81 (30.3)	14 (23.0)		31 (27.9)	9 (31.0)		30(16.9)	11(26.8)	
	Past	43 (16.1)	10 (16.4)		21 (18.9)	8 (27.6)		34(19.2)	9(22.0)	
Smoking index		345.4 (505.5)	396.1 (873)	0.545	351.3 (517.6)	593 (945.1)	0.065	279.5 (488.3)	478 (645.5)	0.070
White blood cell count		8.1 (5.9)	7 (2.8)	0.137	7.5 (3.2)	7.1 (2.1)	0.498	6.9(2.1)	7.2(3.0)	0.095
Neutrophilic granulocyte percentage		44.8 (34)	53.7 (23.3)	0.051	43.9 (34.2)	50.6 (25.6)	0.325	63.4(13.4)	64.5(12.3)	0.112
Percentage of lymphocytes		15.7 (24.1)	20.5 (11.2)	0.127	14.5 (14.5)	17.4 (10.5)	0.316	24.2(9.7)	24.2(13.4)	0.099
Absolute eosinophil count		0.2 (0.2)	0.2 (0.1)	0.137	0.2 (0.2)	0.2 (0.2)	0.230	0.9 (1.1)	0.5(1.0)	0.985
Hematocrit		25.8 (19.7)	33.8 (14.6)	0.003	24.4 (18.3)	31.4 (16.3)	0.061	39.4(4.7)	41.7(4.6)	0.004
Red blood cell distribution width		9 (7.9)	12.3 (12.4)	0.009	8.8 (6.6)	10.2 (5)	0.265	13.2 (0.7)	13.5 (0.6)	0.235
Mean platelet volume		11.4 (10.9)	10.5 (1.1)	0.524	10.9 (1.3)	10.8 (1.1)	0.791	9.8(1.3)	9.8(1.2)	0.239
Globulin		27.4 (4.7)	27.2 (4)	0.782	27.1 (5.2)	29.4 (3.4)	0.022	27.8 (0.8)	27.8 (1.9)	0.213

Note.—Categorical variables are presented as numbers, with percentages in parentheses. Continuous variables are presented as means ± SDs with ranges in parentheses, or as medians with interquartile ranges in parentheses

Table 2 Univariable and multivariable logistic regression analysis

Variable		Univariable Analysis		Multivariable Analysis	
		OR [95% CI]	*P* Value	OR [95% CI]	*P* Value
Age		1.04 [1.01, 1.07]	0.028	1.04 [1.01, 1.08]	0.013
Height		1.02 [0.99, 1.06]	0.213	-	-
Weight		1.02 [0.99, 1.04]	0.198	-	-
Gender (ref = Female)	Male	0.79 [0.34, 1.64]	0.550	-	-
BMI		1.03 [0.95, 1.11]	0.475	-	-
GOLD		1.44 [1.00, 2.08]	0.049	1.43 [0.97, 2.09]	0.068
Hypertension (ref = No)	Yes	0.64 [0.27, 1.36]	0.275	-	-
Diabetes (ref = No)	Yes	0.57 [0.09, 2.09]	0.463	-	-
Smoking index		1.00 [1.00, 1.00]	0.546	-	-
Smoking status (ref = non-smoker)	Current smoker	0.67 [0.33, 1.28]	0.267	-	-
Smoking status (ref = non-smoker)	Ex-smoker	0.90 [0.40, 1.90]	0.788	-	-
White blood cell count		0.92 [0.83, 1.00]	0.105	-	-
Neutrophilic granulocyte percentage		1.01 [1.00, 1.02]	0.053	0.99 [0.97, 1.00]	0.142
Percentage of lymphocytes		1.01 [1.00, 1.02]	0.191	-	-
Absolute eosinophil count		0.19 [0.02, 1.13]	0.125	-	-
Hematocrit		1.02 [1.01, 1.04]	0.004	1.05 [1.02, 1.08]	0.004
Red blood cell distribution width		1.04 [1.01, 1.08]	0.031	-	-
Mean platelet volume		0.84 [0.65, 1.00]	0.17	-	-
Globulin		0.99 [0.93, 1.05]	0.782	-	-
Visual CAC score		1.94 [1.41, 2.66]	< 0.001	1.94 [1.41, 2.66]	< 0.001
Lung radscore		3.30 [2.35, 4.64]	< 0.001	3.14 [2.21, 4.48]	< 0.001
Mediastinum radscore		12.17 [6.32, 23.45]	< 0.001	11.53 [5.84, 22.75]	< 0.001
Combined lung and mediastinum Radscore		12.17 [6.32, 23.45]	< 0.001	11.53 [5.84, 22.75]	< 0.001

Note.—The number of patients with hyperlipidemia in the training set was too small (1/328), and the univariate logistic analysis result was NA

Based on the multivariable logistic regression analysis, age ($p = 0.013$), hematocrit ($p = 0.004$), neutrophilic granulocyte percentage($p = 0.142$) and GOLD ($p = 0.068$) were incorporated into the construction of the clinical factor model. The consistent between the CACS of the two radiologists was 0.95 ($p = 0.000$) by kappa. Visual CACS ($p = 0.000$) was an independent factor in multivariable logistic regression analysis and used as visual CACS model alone.

Consistency assessment between manual and fully automatic segmentation

The mediastinum segmentations were assessed using the Dice index, an objective measure that quantifies the spatial, overlap between two contours. The mean Dice coefficient between manual and automatic segmentation was 0.98 ± 0.02 for mediastinum.

Feature extraction, selection, and radiomics signature construction

1218 whole lung and 1218 mediastinum radiomic features were extracted from CT images. After normalization and deletion of features with correlation greater than 0.9, 230 whole lung, 236 mediastinum and 470 lung-and-mediastinum features remained. After features selection lung, mediastinum, combined lung-and-mediastinum radiomics signatures were constructed using 12(11 Texture features, 1 First-order feature), 6(5 Texture features, 1 First-order feature) and 6(5 Texture features, 1 First-order feature) features, respectively (Fig. 3a, b and c). We found the 6 features of the combined lung-and-mediastinum radiomics model were exactly the same as the 6 features of the mediastinum radiomics model, thus we continued with just using the mediastinum radiomics model. Independent risk factor identification of CVD (univariable and multivariable logistic regression analysis result) is shown in Table 2. The lung radiomics model (OR[95% CI]:3.14 [2.21, 4.48], $p = 0.000$), and the mediastinum radiomics model (OR[95% CI]:11.53 [5.84, 22.75], $p = 0.000$) were independent factors in univariable and

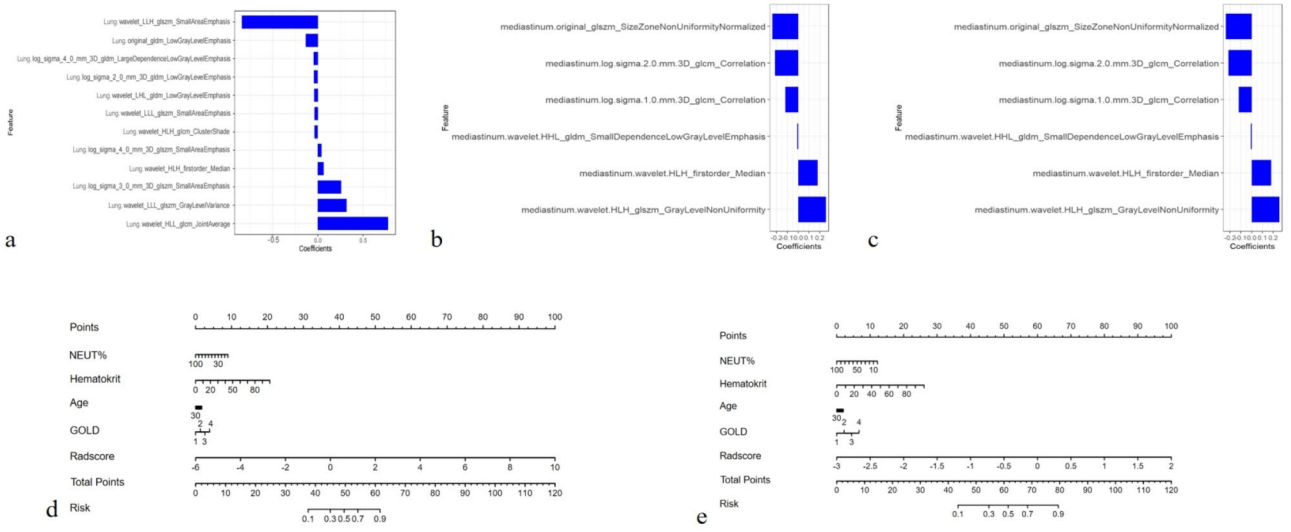

Fig. 3 Radiomics features and corresponding coefficients retained after dimensionality reduction by LASSO regression analysis (**a**: lung radiomics; **b**: mediastinum radiomics; **c**: lung-and-mediastinum radiomics); The developed radiomics nomogram to predict CVD of COPD patients (**d**: lung nomogram; **e**: mediastinum nomogram). NEUT%, neutrophilic granulocyte percentage

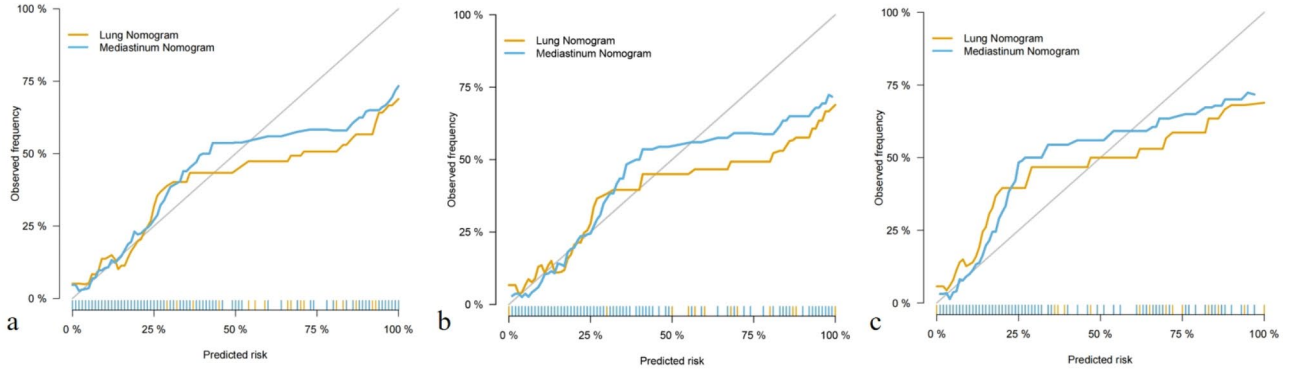

Fig. 4 The calibration curve predicts the CVD of COPD patients. (**a**: training cohort; **b**: internal validation cohort; **c**: external validation cohort)

multivariable logistic regression analysis. The formulas for the radiomics scores are in the supplement.

Development of radiomics nomograms and evaluation of the performance of models

The two radiomics models (lung and mediastinum) were incorporated with the factors of the clinical factors model, comprising age, neutrophilic granulocyte percentage, hematocrit, and GOLD stage, to construct the final combined models, presented as nomograms. The formulas of the nomogram scores are in the supplement. The Hosmer-Lemeshow test showed that the 2 combined models had good calibration ($p = 0.576$, 0.885, and 0.129, 0.441, and 0.059, 0.078, in the training, internal validation, and external validation cohort, respectively). The Brier scores of the lung combined model and mediastinum combined model are 0.112, 0.111, and 0.140, 0.110, 0.128 and 0.136 in the training, internal validation, and external validation cohort, respectively. The nomograms and calibration curves are shown in Figs. 3 and 4.

The diagnostic performance of the clinical factors model, the radiomics models, and the combined models is shown in Table 3. In the training cohort, AUC of the radiomics models and of the combined models was significantly higher than that of the clinical factors model (lung: $p = 0.019$; Mediastinum: $p = 0.000$) and visual CACS model (lung: $p = 0.011$; Mediastinum: $p = 0.000$). Similar trends were found in internal and external validation cohort. In the training, internal and external validation cohorts, the AUC of the mediastinum radiomics model was higher than the visual CACS model ($p = 0.000$; $p = 0.004$; $p = 0.012$). There was no significant difference between lung radiomics model and visual CACS model in the training and external validation cohorts ($p = 0.060$; $p = 0.156$), and there was significant difference in the internal validation cohort ($p = 0.000$). In the training

Table 3 Diagnostic performance of the radiomics model, clinical model, and combined model

Model		AUC [95% CI]	Accuracy (%)	Sensitivity (%)	Specificity (%)	P-value of DeLong-Test			
						vs. Lung Radiomics model	vs. Mediastinum/ Lung-andMediastinum Radiomics model	vs. Lung Combined model	vs. Mediastinum Combined model
Lung Radiomics model	Training cohort	0.76[0.68, 0.83]	90	49	99	-	0.012	0.029	0.003
	Internal validation cohort	0.84 [0.76, 0.93]	88	52	97	-	0.669	0.949	0.893
	External validation cohort	0.69 [0.62, 0.77]	48	93	38	-	0.234	0.189	0.112
Mediastinum/ Lung-and-Mediastinum Radiomics model	Training cohort	0.85 [0.79, 0.91]	85	69	89	-	1	0.081	0.034
	Internal validation cohort	0.82 [0.72, 0.93]	84	66	88	-	1	0.702	0.283
	External validation cohort	0.76 [0.68, 0.84]	63	85	58	-	1	0.527	0.018
Clinical model	Training cohort	0.71[0.64, 0.78]	63	79	59	0.267	<0.001	0.019	<0.001
	Internal validation cohort	0.70 [0.59, 0.81]	63	66	63	0.190	0.056	0.007	0.015
	External validation cohort	0.59 [0.51, 0.68]	39	93	26	0.062	0.005	0.003	<0.001
CAC scores model	Training cohort	0.65 [0.57, 0.72]	77	38	86	0.060	<0.001	0.011	<0.001
	Internal validation cohort	0.58 [0.47, 0.70]	71	32	83	<0.001	0.004	0.002	0.002
	External validation cohort	0.62 [0.53, 0.71]	73	27	84	0.156	0.012	0.047	0.003
Lung Combined model	Training cohort	0.79[0.72, 0.86]	86	56	93	-	-	-	0.021
	Internal validation cohort	0.84 [0.74, 0.94]	86	62	92	-	-	-	0.914
	External validation cohort	0.72 [0.65, 0.80]	60	83	54	-	-	-	0.294
Mediastinum Combined model	Training cohort	0.86 [0.81, 0.92]	83	74	85	-	-	-	-
	Internal validation cohort	0.84 [0.74, 0.94]	79	72	81	-	-	-	-
	External validation cohort	0.78 [0.70, 0.85]	67	78	64	-	-	-	-

Note.—The lung-and-mediastinum radiomics model are exactly the same as the mediastinum model. AUC = Area under the receiver operating characteristic curve

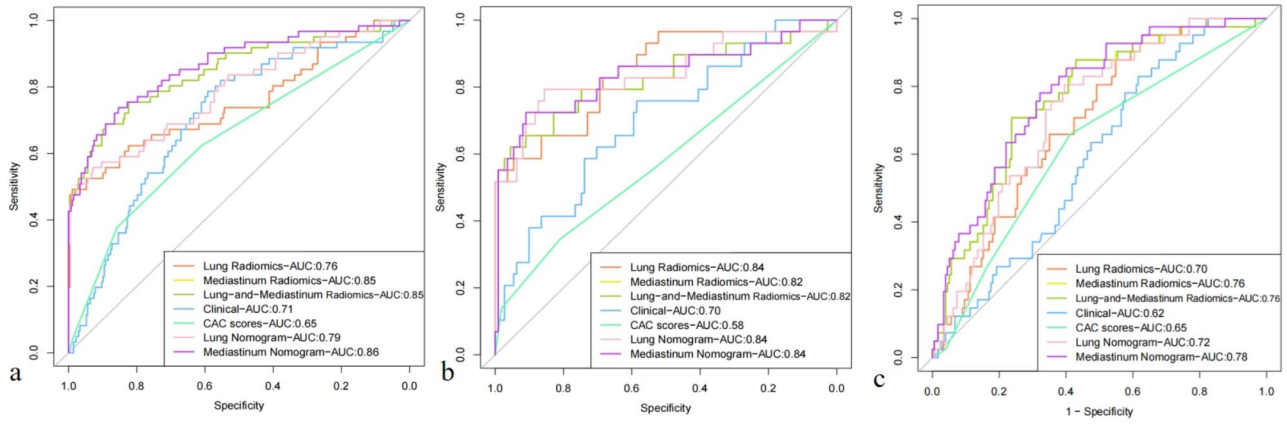

Fig. 5 The ROC curves of the lung, mediastinum radiomics model, clinical model, CAC scores, lung nomogram, and mediastinum nomogarm for predicting CVD of COPD patients in the training cohort (**a**), internal validation cohort (**b**) and external validation cohort (**c**)

cohort, AUC of the mediastinum combined model was significantly higher than that of the lung combined model ($p = 0.021$), but there were no significant differences in AUCs in internal and external validation cohorts. The ROC curves of the models are presented in Fig. 5. Figure S1 shows the decision curve analysis (DCA) for the nomograms. It was observed that the lung (when the threshold probability was > 15%) or mediastinum model (when the threshold probability was > 5%) had a higher overall net benefit in identifying CVD in COPD patients than the clinical factors model and covered most of the range of reasonable threshold probabilities.

Subgroup analyses

The ROC curves for subgroup analyses are shown in Fig. 6. In the COPD population with GOLD stage I-II, the AUC of the lung combined model and mediastinum combined model were 0.69 95%CI [0.57, 0.80] and 0.78 95%CI [0.69, 0.88], respectively. In the GOLD stage III-IV COPD subgroup, both models demonstrated stable

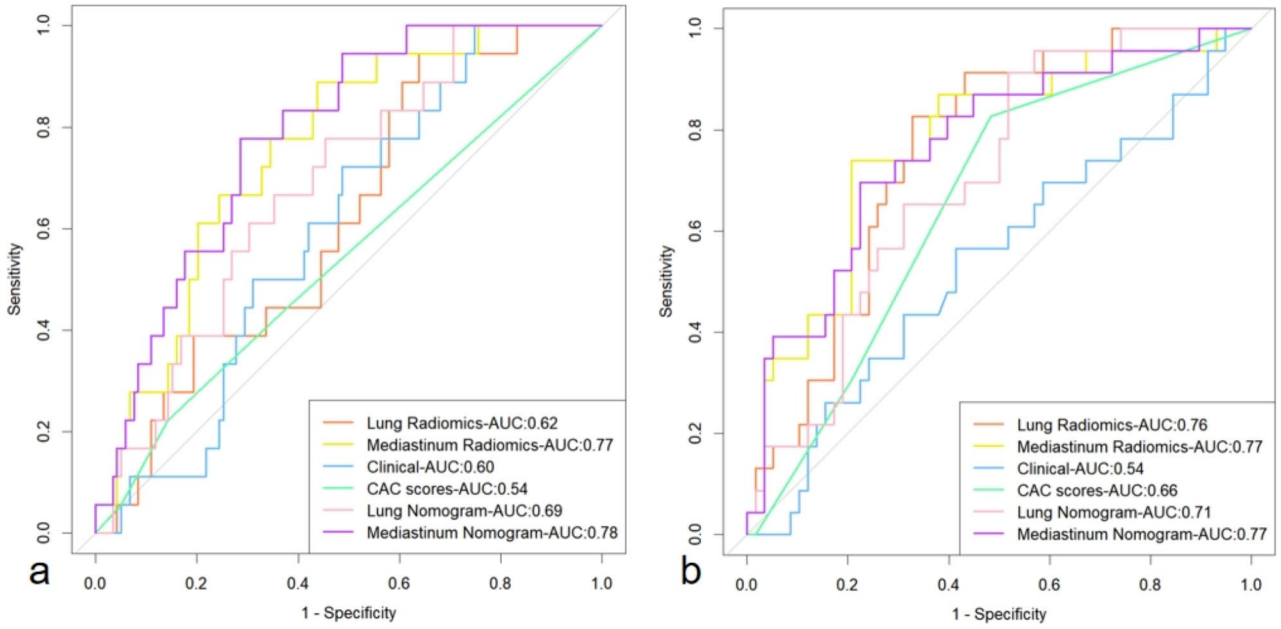

Fig. 6 Subgroup analyses: the ROC curves of the lung, mediastinum nomogram for predicting CVD of COPD patients in the external validation cohort (**a**: GOLD stage I-II, **b**: GOLD stage III-IV)

performance, with AUCs of AUC:0.71 95%CI [0.59, 0.82] for the lung combined model and AUC:0.77 95%CI [0.65, 0.88] for the mediastinum combined model. Notably, the mediastinum combined model consistently achieved the highest performance among all models across different GOLD stage subgroups.

Discussion

The heart and lungs interact functionally, with COPD potentially leading to cor pulmonale [23]. However, cardiac and lung diseases are mostly assessed separately, increasing screening costs and delaying the timeliness of disease management. Based on a one-stop-shop chest CT, this study established and verified the ability of nomograms (lung: 0.79; mediastinum: 0.86) to identify CVD in COPD patients, especially the mediastinum nomogram model, with slightly higher AUC if combined with clinical factors. The two nomograms also showed robust efficacy in subgroup analysis.

In recent years, there have been a number of studies focusing on identifying COPD with coexisting CVD through clinical data. Many studies [24, 25] show that age and gender are independent predictors of CVD in COPD. In our study, gender ($p = 0.550$) was not included in the model construction, possibly because the proportion of women (19.0%) in the cohort was relatively low. However, COPD is more common in men [26]. As discovered in another study [25], waist circumference, and diastolic blood pressure are also independent predictors, and resulted in a model with an AUC of 0.73. In clinical practice, however, most patients with COPD do not have these two records and the AUC is not optimal. Shi et al. [27] constructed a logistic regression model with age, gender, BMI, high-density lipoprotein (HDL), glycosylated hemoglobin, family history of heart disease, and hospitalization due to illness in the last year as the variables, with a slightly better AUC of 0.74. Therefore, it seems better to incorporate more biomarkers to improve the predictive effect of the model. Previous studies [28, 29] have shown that neutrophilic granulocyte percentage and hematocrit are related to CVD such as myocardial infarction and dilated cardiomyopathy. Our study included these two parameters and found that they were valuable for the identification of CVD in COPD patients. Smoking is a common risk factor for COPD and CVD [30, 31]. However, we found that the proportion of smokers was similar for the COPD patients with and without CVD (46.6% vs. 43.2%). This is the reason that smoking status was not included in our model. Yaker et al. [32] identified combined CVD based on a model including the monocytes to HDL-cholesterol ratio, with an AUC of 0.73. The results of studies on clinical factors, as mentioned above, indicate that predicting (presence of) CVD in COPD based on models with only clinical factors is suboptimal. In our study, we constructed 2 models that combined clinical factors and imaging features with better performance.

To our best knowledge, there are few studies for the identification of CVD in patients with COPD using chest CT-based radiomics. According to prior work, coronary calcification, which has been shown to be associated with small pulmonary vascular alteration changes

in COPD [33]. The Weston score, a visual score that scores calcification in each major coronary vessel, correlates well with the quantitative Agatston score and predicts incident CVD in COPD patients with a C index of 0.62 [17, 34]. This performance is similar to that of the CAC model developed in our study, which had an AUC of 0.65 (95% CI: 0.57–0.72). Moreover, our CAC scoring method was more straightforward and easier to implement. Importantly, our study further demonstrated that the nomograms (lung: 0.79; mediastinum: 0.86) outperforms the CAC model in identifying CVD. Additionally, previous studies have primarily focused on identifying CVD risk within the general population. Esmeralda et al. [35] constructed a prediction model for atrial fibrillation based on clinical factors, cardiovascular MRI indices, and radiomics to predict CVD in the general population, with an AUC of 0.76. Pujadas et al. [36]. built an atrial fibrillation prediction model (AUC 0.61) using electrocardiogram markers and cardiac MRI radiomics, and model performance significantly improved with the addition of radiomics. The above studies verified the feasibility of radiomics. However, MRI-based radiomics is costly and less clinically applicable to COPD patients than CT. Furthermore, the models in our study do not require fine annotation of the great vascular regions of the heart, only the mediastinum or the lung is required, which reduces the difficulty of organ segmentation. Importantly, we excluded patients with more easily identifiable signs of coronary artery disease, namely history of coronary stenting and bypass grafting.

Our previous study [15] build a nomogram based on whole-lung CT-based radiomics with clinical factors to identify CVD, with an AUC of 0.73, which was slightly lower than the whole-lung combined model (AUC 0.79) in this study. In contrast, in this study we additionally developed a mediastinum radiomics nomogram, and compared this with a visual CACS model. We found that the lung and mediastinum radiomics models (lung: 0.76; mediastinum: 0.85) performed better than the visual CAC model (AUC: 0.65). Then we combined radiomics model with clinical factors for the next step of model construction. The AUC of the combined model for mediastinum and for lung in the external cohort was 0.78 and 0.72, respectively ($p = 0.294$). Overall, the AUC values for mediastinum combined model were higher than for lung combined model, suggesting that the mediastinum combined model is (even) more applicable for identifying CVD in COPD patients. In this study, lung or mediastinum radiomics model also has good performance, but the AUC is always lower than that of the combined models. Meanwhile, the sensitivity and specificity of the radiomics models were significantly different in the internal and external validation cohorts. This may be related to the relatively higher proportion of patients with severe COPD (GOLD 3, 4) in the external validation cohort (37.2%) than in the internal validation (22.9%) and training (23.8%) cohorts. The higher severity of COPD, the higher risk of CVD [37]. In contrast, the sensitivity and specificity of the combined models were similar among the three cohorts, further indicating the combined model has better stability.

Both lung and mediastinum combined models performed well on the training, internal validation and external validation cohorts (high AUC, good calibration curves), and it can be tentatively assumed that they have some predictive ability. And this is a multicenter study with an independent external validation cohort to ensure its ability to generalize. Prospective trials are the gold standard for validating a model's performance in a real clinical setting. In future studies, small-scale pilot applications of the model in newly hospitalized COPD patients are also needed to assess the predictive performance and clinical utility of the model. And the performance of the model is monitored in real time during the application to ensure that its performance on new data is consistent with the training data, then to optimize the model.

There are some limitations to this study. First, our study was retrospective, and the validity of our model needs to be confirmed in future prospective studies with incidence of CVD events. Second, we could not stratify in the subtypes of CVD due to limited numbers of outcomes. Future studies should expand the sample size. Third, AUC of the combined mediastinum model was no longer significantly higher than the combined lung model in validation cohorts, which is explained by limited outcome numbers. Finally, although aortic valve calcification valve was not analyzed as an independent index in this study, it was included in the mediastinum radiomics analysis as a part of mediastinal structure.

In conclusion, we developed chest CT-based nomograms to identify CVD in COPD patients. The CT-based radiomics models, in particular based on mediastinum features, had better discriminatory power than clinical factors and visual coronary artery calcium score. Studies with prospective CVD outcomes should confirm the clinical applicability of the nomograms.

Supplementary Information

The online version contains supplementary material available at https://doi.org/10.1186/s12890-025-03568-2 .

Supplementary Material 1

Acknowledgements

Grateful to Yayuan Geng (Beijing Shukun Technology Co., Ltd.) for assisting with mediastinum segmentation.

Author contributions
XQ L: Experimental studies; Statistical analysis; Manuscript editing (a major contributor in writing the manuscript). TH Z: Experimental studies; Statistical analysis. J N: Clinical studies. XX Z: Clinical studies. Y G: Literature research. XA J: Literature research. Y X: Literature research. FY X: Clinical studies. HJ H: Clinical studies. J L: Literature research. J Z: Literature research. SY L: Literature research. R V: Manuscript editing. L F: Clinical studies; Manuscript editing. All authors read and approved the final manuscript.

Funding information
This work was supported by the National Key Research and Development Program of China (2022YFC2010002, 2022YFC2010000, 2022YFC2010006 and 2022YFC2010005), the National Natural Science Foundation of China (82171926 and 82430065), the Medical Imaging Database Construction Program of National Health Commission (YXFSC2022JJSJ002).

Data availability
Data generated or analyzed during the study are available from the corresponding author by request.

Declarations

Consent for publication
Not applicable.

Competing interests
The authors declare no competing interests.

Ethics Declarations
This retrospective study was approved by the institutional review boards at Second Affiliated Hospital of Naval Medical University, Tongji Hospital of Tongji University and Sir Run Run Shaw Hospital (Ethical Approval Number: 2022SL068, Data: December 6, 2022; Trial Registration: ChiCTR2300069929, Data: March 29, 2023); no patient informed consent was needed because it was a retrospective study.

Author details
[1]Department of Radiology, Second Affiliated Hospital of Naval Medical University, No. 415 Fengyang Road, Shanghai 200003, China
[2]College of Health Sciences and Engineering, University of Shanghai for Science and Technology, No.516 Jungong Road, Shanghai 200093, China
[3]Department of Radiology, Tongji Hospital, School of Medicine, Tongji University, Shanghai 200065, China
[4]Department of Radiology, Sir Run Run Shaw Hospital, No. 3 Qingchun East Road, Zhejiang 310018, China
[5]Medical imaging international scientific and technological cooperation base of Zhejiang province, Zhejiang 310018, China
[6]Department of Radiology, University Medical Center Groningen, No. 9712 CP, Groningen 9613, The Netherlands

Received: 27 November 2024 / Accepted: 24 February 2025
Published online: 15 March 2025

References

1. Claus F, Vogelmeier F W F, Patrick T, Nils K. Impact of COPD on mortality: An 8-year observational retrospective healthcare claims database cohort study [J]. respiratory medicine, 2023.
2. Jiaxin Xu Z J, Peng Z, Tao C. Disease burden of COPD in the Chinese population: a systematic review [J]. Ther Adv Respir Dis, 2023, 17.
3. Chen S, Kuhn M, Prettner K et al. The global economic burden of chronic obstructive pulmonary disease for 204 countries and territories in 2020-50: a health-augmented macroeconomic modelling study [J]. Lancet Glob Health, 2023, (2214-109X (Electronic)).
4. Xiao-Fang Li C-Q W, Yi-Min M. Analysis of pathogenesis and drug treatment of chronic obstructive pulmonary disease complicated with cardiovascular disease [J]. Frontiers in Medicine; 2022.
5. Peter Alter A R J B, Henrikwatzc T. Left ventricular volume and wall stress are linked to lung function impairment in COPD [J]. Int J Cardiol, 2018.
6. Hong Chen XL, Yuejun DU, Chenyun HE. Association between chronic obstructive pulmonary disease and cardiovascular disease in adults aged 40 years and above: data from NHANES 2013–2018 [J]. BMC Pulmonary Medicine; 2023.
7. Brassington K, Selemidis S, Bozinovski S et al. New frontiers in the treatment of comorbid cardiovascular disease in chronic obstructive pulmonary disease [J]. Clin Sci (Lond) 2019, (1470–8736 (Electronic)).
8. Jelle C.L. Himmelreich LV, Wim AM, Lucassen RS. Prediction models for atrial fibrillation applicable in the community: a systematic review and meta-analysis [J]. Europace, 2020.
9. Peter Flueckiger WL, David H, Joseph Y. Revised Framingham Stroke Risk Score, Non-Traditional Risk Markers, and Incident Stroke in a Multi-Ethnic Cohort [J]. Stroke, 2018.
10. Joseph EAZG, Jennifer KQ, Richard R. QRISK3 underestimates the risk of cardiovascular events in patients with COPD [J]. Thorax. 2023;79(8):718–24.
11. Philippe Lambin RTHL, Timom D, Jurgen P. Radiomics: the Bridge between medical imaging and personalized medicine [J]. Clinical Oncology; 2017.
12. Taohu ZM, Peng W, Dong SD. CT-Based radiomic nomogram for the prediction of chronic obstructive pulmonary disease in patients with lung cancer [J]. Acad Radiol. 2023;30(12):2894–903.
13. Wenjun Huang HD, Zhaobin LI, Zhanda X, Taohu ZM, Wenting TU, Peng MS, Shaofeng D. Baseline whole-lung CT features deriving from deep learning and radiomics: prediction of benign and malignant pulmonary ground-glass nodules [J]. Frontiers in Oncology; 2023.
14. Wenjun Huang H Z, Yanming GE, Shaofeng D. Radiomics-based machine learning methods for volume doubling time prediction of pulmonary Ground-glass nodules with baseline chest computed tomography [J]. J Thorac Imaging; 2023.
15. Lin X, Zhou T, Ni J, et al. CT-based whole lung radiomics nomogram: a tool for identifying the risk of cardiovascular disease in patients with chronic obstructive pulmonary disease [J]. Eur Radiol. 2024;34(8):4852–63.
16. Singhvi D. CT imaging and comorbidities in COPD: beyond lung Cancer screening [J]. Chest. 2021;159(1):147–53. (1931–3543 (Electronic)).
17. Bhatt SP, Kazerooni EA, Newell JD JR, et al. Visual estimate of coronary artery calcium predicts cardiovascular disease in COPD [J]. Chest. 2018;154(3):579–87. (1931–3543 (Electronic)).
18. Labaki WW Rosenberg SR. Chronic obstructive pulmonary disease [J]. Ann Intern Med. 2020;173(3):ITC17–32.
19. Halpin DMG, Criner G J, Papi A, et al. Global initiative for the diagnosis, management, and prevention of chronic obstructive lung disease. The 2020 GOLD science committee report on COVID-19 and chronic obstructive pulmonary disease.[J]. Am J Respir Crit Care Med. 2021;203(1):24–36.
20. Chiles C, Duan F, Gladish G W et al. Association of coronary artery calcification and mortality in the National lung screening trial: A comparison of three scoring methods [J]. Radiology, 2015, (1527– 1315 (Electronic)).
21. Zhou T-H, Zhou X-X, Ni J et al. CT whole lung radiomic nomogram: a potential biomarker for lung function evaluation and identification of COPD [J]. Military Med Res, 2024, 11(1).
22. Wasserthal J, Breit H C, Meyer M T, et al. TotalSegmentator: robust segmentation of 104 anatomic structures in CT images [J]. Radiol Artif Intell. 2023;5(5):e230024.
23. Ramalho SHR S A. Lung function and cardiovascular disease: A link [J]. Trends Cardiovasc Med. 2021, (–1873–2615 (Electronic)):–93–8.
24. Yuanjie QIU Y, Nirui Shen Qingting W. Nomograms for predicting coexisting-cardiovascular disease and prognosis in chronic obstructive pulmonary disease: A study based on NHANES data [J]. Can Respir J 2022.
25. Lee SJ, Yoon S A-O X, Lee MH et al. Health-Screening-Based chronic obstructive pulmonary disease and its effect on cardiovascular disease risk [J]. J Clin Med, 2022, (2077–0383 (Print)).
26. Zhao X A-O, Kang H, An Y et al. Whole-course management of chronic obstructive pulmonary disease in primary healthcare: an internet of things-enabled prospective cohort study in China [J]. BMJ Open Respir Res, 2024, (2052–4439 (Electronic)).
27. Yun Shi J Z, Yingshuo H. Prediction of cardiovascular risk in patients with chronic obstructive pulmonary disease: a study of the National health and nutrition examination survey database [J]. BMC Cardiovasc Disord. 2021;21(1):417.
28. Huang F, Zhang J, Zhou H et al. B cell subsets contribute to myocardial protection by inducing neutrophil apoptosis after ischemia and reperfusion [J]. JCI Insight, 2024, (2379–3708 (Electronic)).

29. Huang Y, Li L C, Li Y X et al. Development and validation of a risk model for intracardiac thrombosis in patients with dilated cardiomyopathy: a retrospective study [J]. Sci Rep, 2024, (2045–322 (Electronic)).
30. Minhas A M K S R, Jean E D, Shapiro M D, Panza J A, Alam M, Virani S S, Ballantyne C M Abramov D. Global burden of cardiovascular disease attributable to smoking, 1990–2019: an analysis of the 2019 global burden of disease study [J]. Eur J Prev Cardiol, 2024, (2047–4881 (Electronic)).
31. PetriE K A M, George J. Smoking, respiratory symptoms, lung function and life expectancy: A longitudinal study of ageing [J]. Respirology, 2024, (1440–843 (Electronic)).
32. Yakar HI, Kanbay A. Could monocyte level/hdl cholesterol ratio predict cardiovascular diseases in patients with COPD? [J]. Niger J Clin Pract, 2023, (1119–3077 (Print)).
33. Matsuoka S, Yamashiro T, Fau-Diaz A, Diaz A Fau - ESTéPAR RSJ, et al. The relationship between small pulmonary vascular alteration and aortic atherosclerosis in chronic obstructive pulmonary disease: quantitative CT analysis [J]. Acad Radiol. Jan; 2011;18(1):40–6. (1878–4046 (Electronic)).
34. Perone F A-O, Bernardi M A-O, Redheuil A, et al. Role of cardiovascular imaging in risk assessment: recent advances, gaps in evidence, and future directions. [J]. J Clin Med. 2023;26(17):5563. (2077– 0383 (Print)).
35. Esmeralda Ruiz Pujadas Z R-E, Liliana S, Celeste M. Prediction of incident cardiovascular events using machine learning and CMR radiomics [J]. Eur Radiol, 2022.
36. Esmeralda Ruiz Pujadas Z R E, Liliana S. CRISTIAN IZQUIERDO MORCILLO. Atrial fibrillation prediction by combining ECG markers and CMR radiomics [J]. Curr Opin Pulm Med; 2022.
37. Whittaker H R, Bloom C. Morgan A. Accelerated FEV1decline and risk of cardiovascular disease and mortality in a primary care population of COPD patients [J]. Eur Respir J, 2021, 57(3).

Publisher's note